We are IntechOpen, the world's leading publisher of Open Access books
Built by scientists, for scientists

5,000
Open access books available

125,000
International authors and editors

140M
Downloads

Our authors are among the

154
Countries delivered to

TOP 1%
most cited scientists

12.2%
Contributors from top 500 universities

CLARIVATE ANALYTICS
BOOK CITATION INDEX
INDEXED

WEB OF SCIENCE™

Selection of our books indexed in the Book Citation Index
in Web of Science™ Core Collection (BKCI)

Interested in publishing with us?
Contact book.department@intechopen.com

Numbers displayed above are based on latest data collected.
For more information visit www.intechopen.com

The High-Speed 6xxx Aluminum Alloys in Shape Extrusion Industry

Rafał Hubicki and Maria Richert

Abstract

This chapter describes and analyzes the 6xxx aluminum alloys used in the shape extrusion sector dedicated to automotive and construction industry. The division and application of 6xxx aluminum alloys are performed. The precipitation hardening of **6xxx** (Al-Mg-Si) alloys is presented as these alloys easily undergo deformation and present the potential for new kinds of alloys for high-speed extrusion. The mechanisms of strengthening are shown with the evolution of precipitation sequences. Also some examples of industry applications of 6xxx aluminum alloys are presented.

Keywords: aluminum alloys, extrusion, aging, microstructure

1. Characteristics of aluminum alloys

Historically, aluminum was first produced in 1825 by reducing aluminum chloride with potassium amalgam. In 1886, Héroult and Hall discovered the possibility of producing aluminum by electrolysis. In 1895, aluminum was first used as a material for the church roof. With the increase in the production of aluminum, which occurred especially after the Second World War, the scope of its use expanded. Today, aluminum alloys are widely used in transport, mechanical engineering, electrical and energy industries, food industry, chemical industry, sports, aviation, transport, yacht and shipbuilding, and many other fields. Below, in **Table 1**, the grades of aluminum alloys used in industry are presented.

Group	Series	Alloy
Al	1xxx	1050A, 1070A
Al-Cu	2xxx	2014, 2017, 2024
Al-Mn	3xxx	3103, 3003
Al-Mg-Si	6xxx	6060, 6063, 6061, 6082
Al-Si	4xxx	4032
Al-Mg	5xxx	5019, 5083, 5754
Al-Zn	7xxx	7003, 7020, 7022, 7075

Table 1.
Industrial aluminum alloy groups.

Aluminum alloys are highly ductile, so it is easy to make the desired structural elements, machine parts, and others from them.

By changing the content of alloying elements in aluminum alloys, the strength properties can be adjusted. A very effective factor influencing the strengthening of aluminum alloys is heat treatment—supersaturation and aging. This treatment is possible for Al-Mg-Si 6xxx series alloys, which show a variable solubility in the solid state. Similar possibilities are also available for the 2xxx, Al-Cu-Mg, and 7xxx, Al-Zn-Mg-Cu, alloys (**Figures 1** and **2**). However, the most popular alloy for profile extrusion is 6xxx series.

During the extrusion process, aluminum alloys are placed in the extrusion press container (cylinder) and pressed by a pressing ram (or stem—via a dummy block or pressure plate). The metal flows out through the hole in the die, which gives the shape to the extruded profile (**Figure 3**).

The state of stress in most of the plasticized area is a three-axial nonuniform compression. It is therefore possible to make large plastic deformations without affecting the consistency of the material (maximum elongation coefficients are about 300, average—about 50). This is the main advantage of extrusion processes. Large deformations require high forces. The main limitation to the scale of deformation that can be obtained in one extrusion operation is not the phenomenon of material decohesion (as in many other processes) but the strength of the tools.

When the extruded section leaves the tool, it is cooled with water or air and then drawn, still in the malleable state. This removes the stresses accumulated in the aluminum alloy and at the same time allows to achieve the expected and correct profile dimensions. The profiles are then cut and obtain ultimate strength by hot or cold hardening.
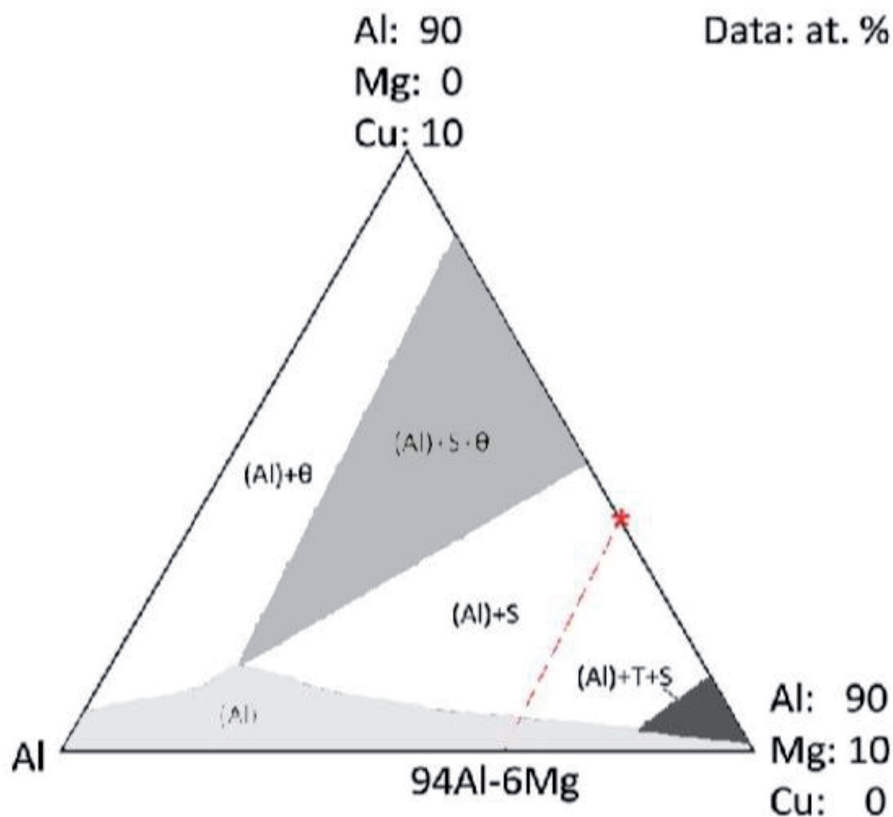

Figure 1.
Isothermal section of ternary Al-Cu-Mg phase diagram at 400°C, h ¼ CuAl 2, S¼ MgCuAl 2, and T ¼ (Cu 1-x Al x) 49 Mg 32. Along the dashed red line, the atomic fraction is constant, 94Al-6 Mg. And at the red star, the composition point is 90Al-4Cu-6 Mg, namely, the average composition of the eutectic region, shown with the dashed white box.
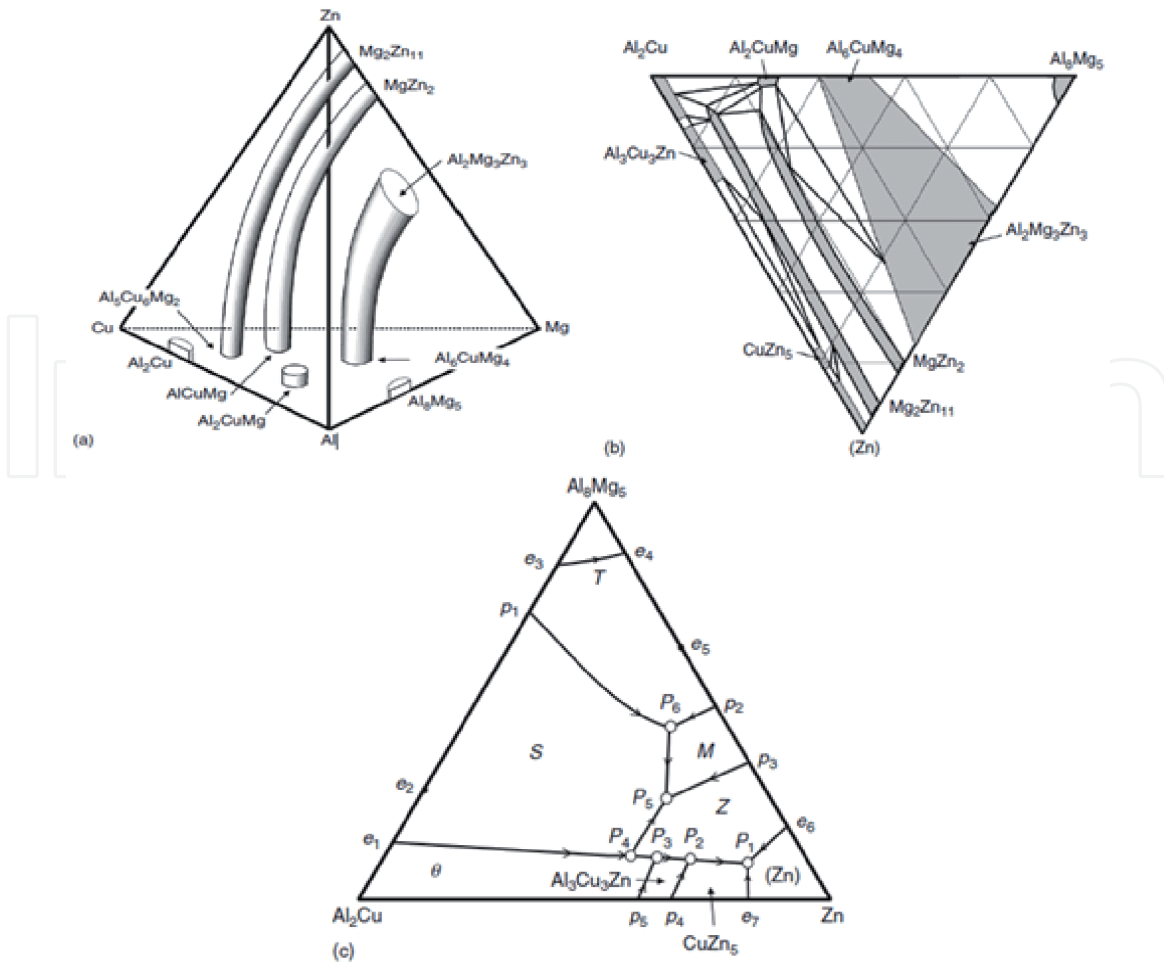
Figure 2.
Phase diagram Al-Cu-Mg-Zn: (a) polythermal diagram, (b) distribution of phase fields in the solid state in the aluminum corner, and (c) single-phase domains [1].
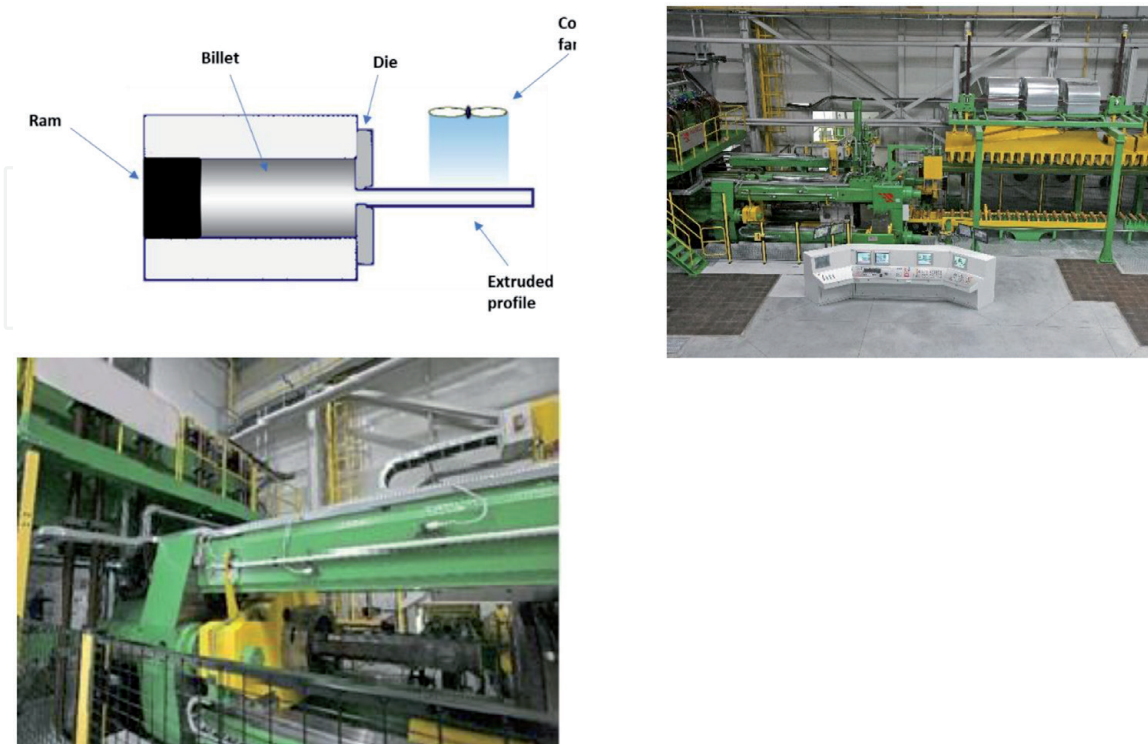

Figure 3.
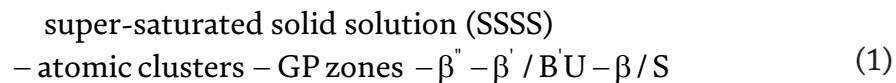*Extrusion diagram and extrusion press for aluminum alloys.*

In the case of large strains, hot extrusion is used, because during cold extrusion the forces are so high that the tools do not withstand the loads. Cold extrusion for large deformations can only be performed for soft materials (e.g., pure aluminum).

2. 6xxx series aluminum alloys for extrusion of shapes

The 6xxx series alloys are the most commonly used and their global consumption is the largest. The worldwide demand for aluminum is around 29 million tons per year. About 22 million tons is new aluminum and 7 million tons is recycled aluminum scrap. The use of recycled aluminum is economically and environmentally compelling. It takes 14,000 kWh to produce 1 ton of new aluminum. Conversely, it takes only 5% of this energy to remelt and recycle 1 ton of aluminum. There is no difference in the quality between virgin and recycled aluminum alloys [2].

Alloys of the 6xxx series are heat-treated as they show a variable solubility in the solid state. **Figure 4** shows a pseudo-binary system Al-Mg$_2$Si. The variable solid solubility curve allows for heat treatment of 6xxx series alloys. After plastic working (e.g., extrusion), the supersaturation and artificial aging of these alloys are applied. After supersaturation, which consists in rapid cooling of the alloy, it is then heated to an appropriate temperature in order to precipitate hardening phases.
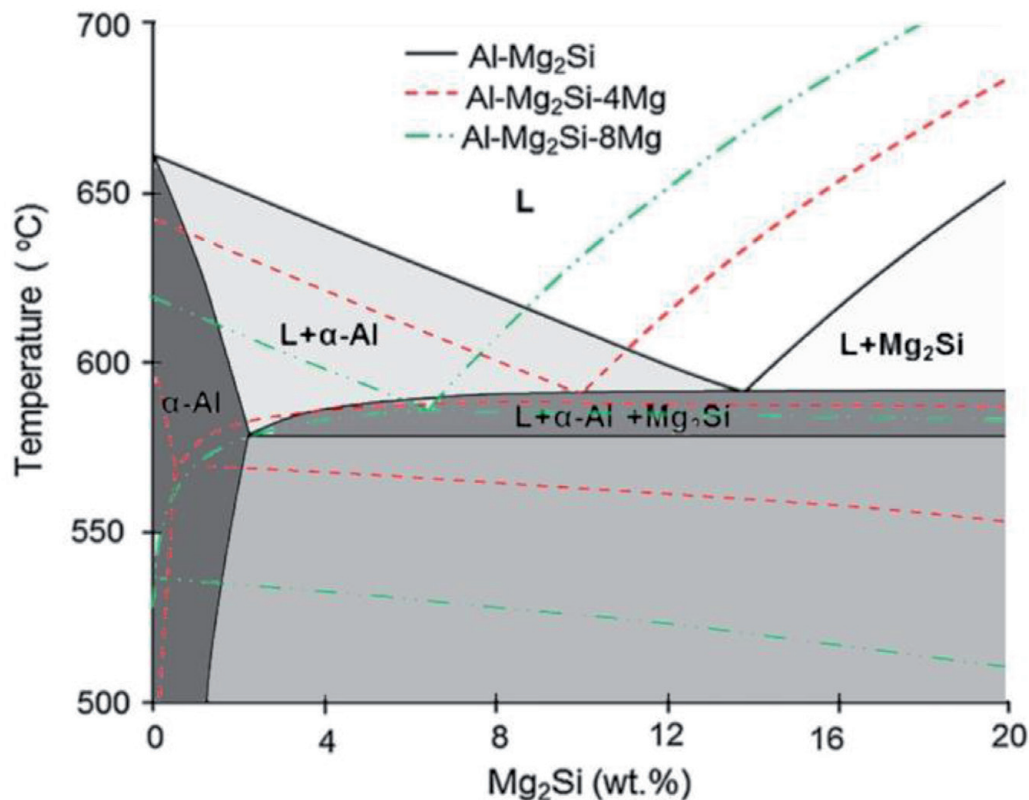
The phase sequence in this alloy is as follows:

$$\text{super-saturated solid solution (SSSS)} - \text{atomic clusters} - \text{GP zones} - \beta'' - \beta' / B'U - \beta / S \tag{1}$$

5

Figure 4.
Calculated equilibrium phase diagram of Al-Mg2Si pseudo-binary alloys with excess Mg.

Phase	Phase form	Formula	Spatial group	Network parameters
GP zones [4, 5]	Needles	Unknown	C2/m	a = 1.48, b = 0.405, c = 0.648, β = 105.3 deg
β″ [6, 7]	Needles	Mg_5Si_6	C2/m	a = 1.516, b = 0.405, c = 0.674, β = 105.3 deg
β′ [8, 9]	Needles	$Mg_{1.8}Si$	$P6_3$	a = b = 0.715, c = 0.405, γ = 120 deg
U1 [8, 10–12]	Needles	$MgAl_2Si_2$	P_{3m1}	a = b = 0.405, c = 0.674, γ = 120 deg
U [8–12]	Needles	MgAlSi	P_{nma}	a = 0.675, b = 0.405, c = 0.794
B [10]	Lath	Unknown	Hexagonal	a = 1.04, c = 0.405, γ = 120 deg
β	Plates	Mg_2Si	F_{m3m}	a = 0.6354
Si	Plates	Si	F_{d3m}	a = 0.5431

Table 2.
Precipitations in 6xxx series alloys.

Table 2 describes the characteristics of the precipitating phases [3].

Si plates appear in silicon-rich alloys. All phases that show the shape of needles are consistent with the direction <100> of the aluminum matrix.

The extrusion temperature of Al-Mg-Si alloys ranges between 400°C and 500°C, which causes that all phases are dissolved in the alloy to form a solid solution. Therefore, in order to prevent the precipitation of an incoherent phase of Mg_2Si, a rapid quenching of the alloy is required after extrusion.

Rapid quenching maintains the supersaturation of the alloy's solid solution caused by Mg and Si and a high concentration of vacancies, also resulting from rapid cooling. The supersaturation is followed by the aging process (**Figure 5**). It is carried out at temperatures from 165°C to 185°C until maximum hardness is reached—state T6.

Hardening achieved as a result of aging depends on the size and density of the precipitations and the volume of metastable phases obtained.

Isothermal heating at 175°C induces the precipitation of β-phase hardening the alloy. The β″-phase is the most effective hardening phase in Al-Mg-Si alloys and is
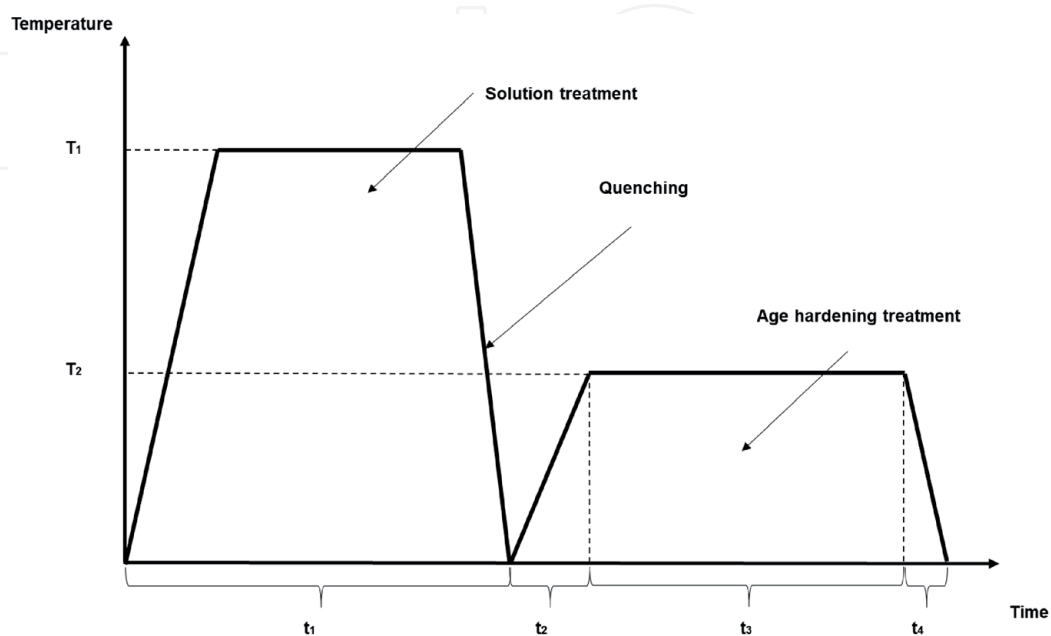

Figure 5.
Sketch of precipitation hardening phases.

formed at temperatures between 125°C and 200°C. The β''-phase composition is Mg_5Si_6; therefore, an appropriate Mg/Si ratio of 5/6 should be maintained during the casting process. The β-phase (Mg_2Si) is not formed below 200°C, so it cannot be present in alloys aged below this temperature.

Marioara et al. [3] studied phase β'' precipitation at different Mg/Si ratios. The research showed that a higher Si content in the alloy promotes the formation of a large number of fine GP zones in a shorter time than alloys with a lower Si content. After annealing for 3 h at 175°C, there was a sharp peak of hardness associated with the appearance of GP zones in these alloys, and after 17 h, a wider peak of hardness associated with the occurrence of phase β'' precipitation appeared. Alloys richer in Mg had thicker elements of microstructure than alloys with an increased Si content. They also contained less U2 precipitations but were richer in β′ precipitations. The studies carried out revealed a strong influence of Si, the content of which controls the process of phase precipitation through the formation of precipitation clusters in the initial stages of annealing.

The great interest in Al-Mg-Si alloys is related to their application in the automotive industry. Chakrabarti et al. [13] conducted a research proving that the strengthening phase involved in the Al-Mg-Si ternary alloys is the metastable β'' phase [14, 15].

Kuroda et al. studied the effect of small amounts of Ni, Co, and V on hardness after age hardening of the AlMgSi base alloy. It was found that the additives increase the hardness, with the highest value of hardness occurring after the introduction of Ni and two-stage aging [16].

The influence of Cu addition on the precipitation process in AlMgSi alloy was studied by Zandbergen et al. [17]. The occurrence of Cu in all investigated precipitations of the hardening phases of the alloy was determined.

On the other hand, the influence of Zn and Ag additives on the precipitation process in AlMgSi alloys was analyzed in the work of Saito et al. [18]. The researchers found a weak influence of Zn on the precipitation sequence of hardening phases. They found that Zn is built into the structure of precipitations replacing some elements in the network of precipitated phases.

A new alloy based on AlMgSi, with the addition of Mn that did not require aging after extrusion, was presented by Lee et al. [19]. Mn creates precipitations of 0.05–0.5 μm. The alloy containing 1 wt.% Mn had high strength properties and good ductility in comparison with the commercial 6N01 alloy. Moreover, it showed higher fatigue resistance.

Chen et al. studied the process of phase precipitation in Al-Mg-Si alloys [20]. They showed that the formation of Mg_5Si_6, hardening AlMgSi alloy, is preceded by the precipitation of $Mg_2Si_{2,6}Al_{6,4}$ and more precisely $Mg_2Si_2Al_7$. The precipitation of this phase is dependent on the temperature of the aging of the alloy.

Mechanisms of hardening with β'' particles, characterized by coherence with aluminum network, were studied by Ringdalen et al. [21]. The study concerned the alloy 6060 and included the interaction of the dislocation lattice with the precipitations.

The AlMgSi alloy, due to the possibility of heat treatment, has a high potential for modeling its structures and properties. Analyzing the process of supersaturation of this alloy and subsequent aging, it is possible to obtain the assumed properties. Hardening phases in the AlMgSi alloy nucleate heterogeneously at the grain boundaries and iron precipitations, which are always present in AlMgSi alloys
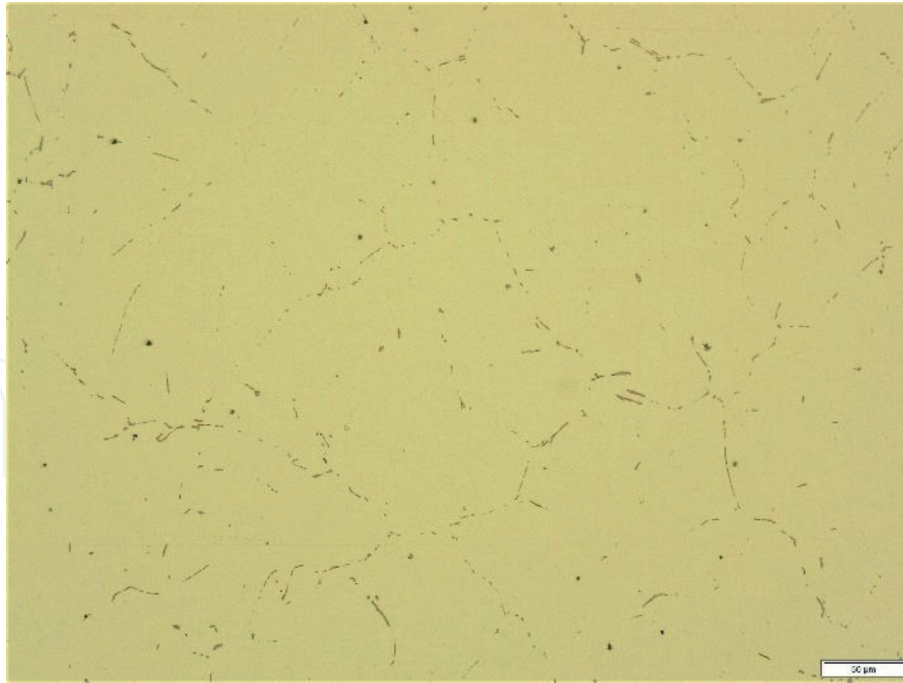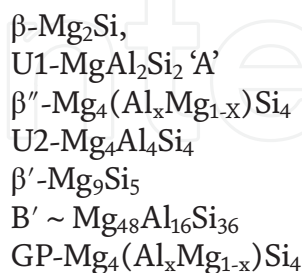
Figure 6.
Hardening phases in AlMgSi alloy.

(**Figure 6**). Precipitations of β'', the hardening phase of AlMgSi alloy, can be found at **Figure 7**. Their growth to larger sizes is associated with the formation of Mg_2Si phase. Large Mg_2Si particles are not an obstacle to displaced dislocations and do not increase the strength properties of the alloy.

An example of research on the heat treatment of AlMgSi alloys is the article by Richert et al. [22] concerning the new, multistage aging of the 6xxx series alloys. The studies of Ryen et al. [23] showed the presence in alloys AA6063 and AA6068, after aging precipitations as B', β'', U2, and U1, β' and some unidentifiable crystal structures. Detailed studies of the precipitations in aluminum alloys are also presented in the work by Andersen et al. [24]. From this work, data were taken from the composition of the precipitations formed during aging in AlMgSi alloys:

β-Mg_2Si,
U1-$MgAl_2Si_2$ 'A'
β''-$Mg_4(Al_xMg_{1-x})Si_4$
U2-$Mg_4Al_4Si_4$
β'-Mg_9Si_5
B' ~ $Mg_{48}Al_{16}Si_{36}$
GP-$Mg_4(Al_xMg_{1-x})Si_4$

The author found that the early stages in Al-Mg-Si and Al-Mg-Cu systems have isostructural GP zones being 1D strings along <100>Al, identical to the eye-like units of the β''-phase, where Cu can replace Si. Calculations show GP zones can take different compositions, the most stable being Mg_4Si_4Mg and Mg_4Cu_4Al, with Mg and Al as central interstitial columns. Solute clusters for the GP zones are likely short defect-free needles using a vacancy to produce a central interstitial column. The needle-shaped β''-phase is the most important hardening precipitate in the AA6xxx system.
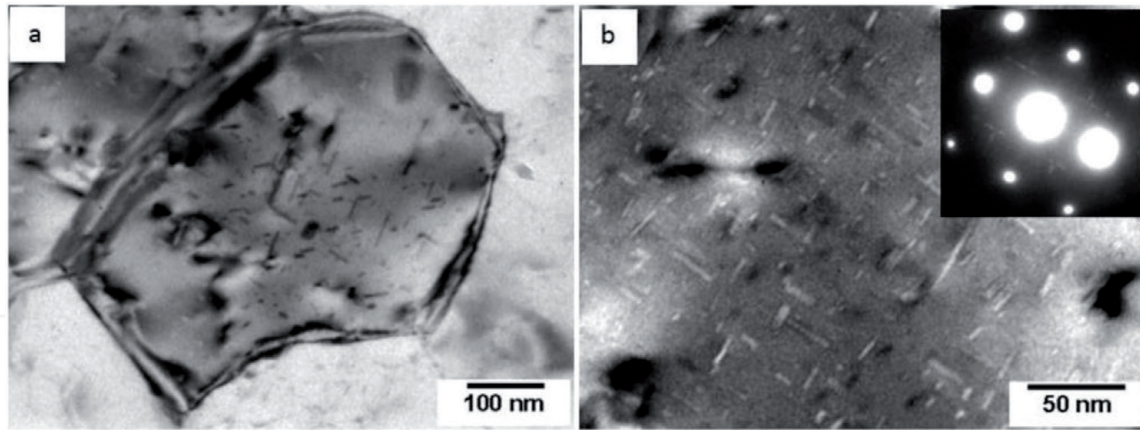
Figure 7.
Nanometric precipitations in AlMgSi alloy [25].

3. High-speed aluminum alloy

3.1 Studies on the production of a high-speed extrusion alloy

3.1.1 Research methodology

In this work, tests were carried out on 6060 alloy with three different chemical compositions, falling within the definition of the standard EN-AW 755-2 (**Table 3**).

Alloy 1 with the lowest Si and Mg contents, Alloy 2 with medium Si and Mg contents, and Alloy 3 with the highest Si and Mg contents were prepared as follows (**Figure 8**):

1. The billets were continuously cast from 6060 alloy, with a diameter of 228 mm, from three melts, differing in the content of alloying components:

    - Alloy 1 (low alloying content)

    - Alloy 2 (with medium content of alloying elements—standard composition)

    - Alloy 3 (high alloying content)

2. The billets were homogenized in accordance with the technology used in Grupa Kęty S. A.

3. The extrusion of profiles (four-hole die) was performed on a 35 MN press as follows:

    - From each alloy, three billets were extruded with the standard speed of the extrusion ram for this shape, and three billets with the extrusion ram speed increased by 20%.

    - The temperatures of the extrusion billets and the press container were the same for all billets.

    - All extruded sections were saturated on the press runout table and then artificially aged in the furnace to T66.

    - Three samples of each extruded section were taken for each hole to check the strength properties and material hardness of the sections.

	Si	Fe	Cu	Mn	Mg	Cr	Ni	Zn	Ti
Alloy 1	0.38	0.20	0.01	0.04	0.36	0.01	0.01	0.02	0.02
Alloy 2	0.45	0.22	0.01	0.04	0.40	0.01	0.01	0.02	0.01
Alloy 3	0.49	0.21	0.01	0.05	0.45	0.01	0.00	0.01	0.02

Table 3.
Chemical composition of billets tested.

Figure 8.
Aluminum alloy billets before loading onto the loading ramp of the press [26].

The tests of mechanical properties of extruded sections were carried out on the Zwick Z300 fatigue tester.

1. In the second stage, only Alloy 1 was tested as promising the highest ductility and thus the possibility to use the highest extrusion rate for the manufactured sections.

The following tests were carried out:

- Alloy 1 was extruded with the following set speed rates: standard (7 billets); standard + 20% (7 billets); standard + 30% (8 billets); standard + 40% (7 billets); standard + 50% (9 billets); and standard + 60% (9 billets),

- The temperatures of extrusion billets and the container were the same for all variants of extrusion.

- From each extruded shape according to each variant of the ram speed, 12 samples with 1000 mm length (72 samples in total) were taken in order to check the strength properties and for hardness measurement.

- All extruded sections were saturated on the runout of the press and then subjected to different variations of artificial aging to T66.

- After extrusion of the sections and their heat treatment, the yield point and tensile strength of the samples were determined on the Zwick Z300 fatigue tester, and hardness tests were carried out on the Zwick ZHU250 testing machine.

- On the basis of the results presented in **Table 4** and the results of properties tests, the aging variant to achieve the properties of the alloy, according to PN-EN 755-2,2016-05 standard, was selected.

- After extrusion and aging, hardness tests were performed on the Zwick ZHU250, and the yield point and tensile strength were determined on the Zwick Z300 fatigue tester machine.
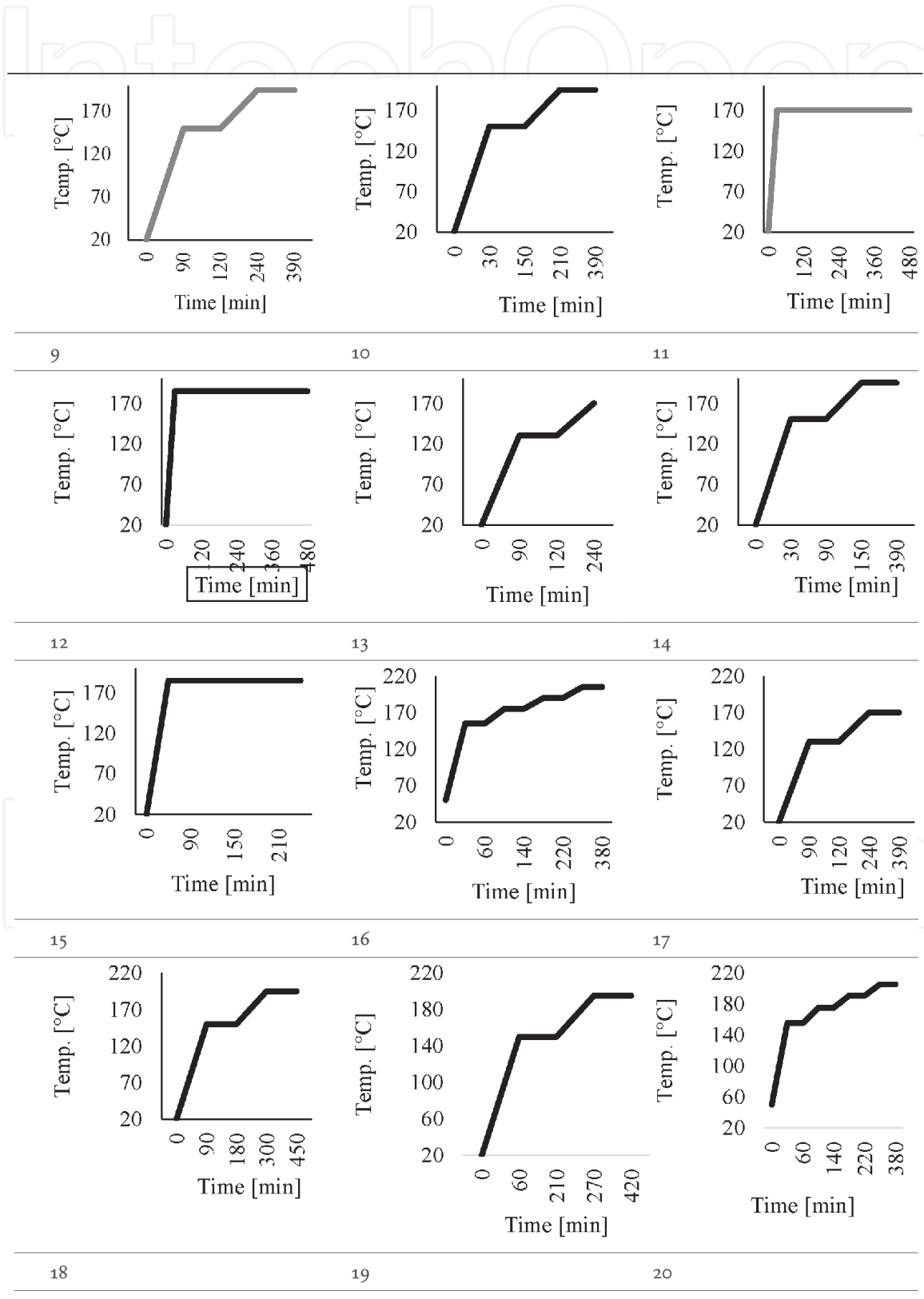

Table 4.
Aging curves of Al-Mg-Si alloy with the lowest composition of alloying elements, second stage of research.

- Observations of the sample structure on the Olympus GX53 and Olympus GX71 and GX51 optical microscopes with digital image capture were performed.

- Samples for microscopic examination and microhardness testing were mounted in the EpoFix epoxy resin. The samples prepared in this way were subjected to grinding (on abrasive papers with the following grades: 220, 500, 800, 1200, 2000, and 4000) and two-stage mechanical polishing according to Struers' procedure using a diamond-paste suspension DiaDuo with a grain size of 3 μm and a colloidal silicon oxide suspension OPS for finish polishing with a grain size of ¼ μm.
Two methods of etching were used:

1. Etching in 0.5% HF acid solution—this method highlights the particles present in the microstructure.

2. Anodizing in Barker's reagent composed of 1.8 ml HBF_4 + 100 ml H_2O—color contrast was obtained from individual grains during polarized light observation.

- Microhardness measurements were performed using the Vickers method with the SHIMADZ HMV-G hardness tester. Microhardness tests were carried out on metallographic specimens at a load of 100 g (HV0.1), and the time to withstand the load was 10 s.

- Observations of the microstructure and morphology of the precipitations with the scanning electron microscope JEOL JSM-6460LV were also performed, using the EDS microanalyzer.

- The share of Mg_2Si phase in the tested samples was determined using the X-ray method. X-ray examinations were performed on PANalytical Empyrean polycrystalline diffractometer with Cu Kα1 = 1.5417 Å, at U = 40 kV and I = 30 mA, equipped with PANalytical High Score Plus program integrated with ICDD PDF4+ 2016 crystallographic database. PIXcel detector was used in the tests. The test range was 10–120° of 2θ angle.

- In the third stage of experimental testing, Alloy 1 was subjected to different aging variants in order to answer the question on which aging variant allows to achieve the assumed alloy properties, compliant with the standard, despite the lowest values of Mg and Si components. The evaluation of the properties of the samples after aging was performed by hardness and microhardness measurements.

3.1.2 Comparative results of tested alloys

The research revealed that after casting and homogenization, Alloy 1 has a correct structure with equiaxed grains and broken lattices of iron precipitations (**Figure 9**).

Figure 10 shows the yield point ($R_{0.2}$) and tensile strength (Rm) of extruded profiles made of Alloy 1 with the lowest alloying content and other alloy compositions with higher content of alloying elements, i.e., Alloy 2 and Alloy 3. According to the requirements of the standard, the extruded section should have minimum $R_{0.2}$ = 160 MPa and Rm = 215 MPa. The shape made of Alloy 2 with the average content of alloying elements and Alloy 3 with the highest content of alloying elements obtained the property level required by the standard EN755-2 (for products made of alloy 6060, in the T66 state). The properties of Alloy 3 are too high. And the shape with the lowest level of alloying elements failed to obtain such a level.
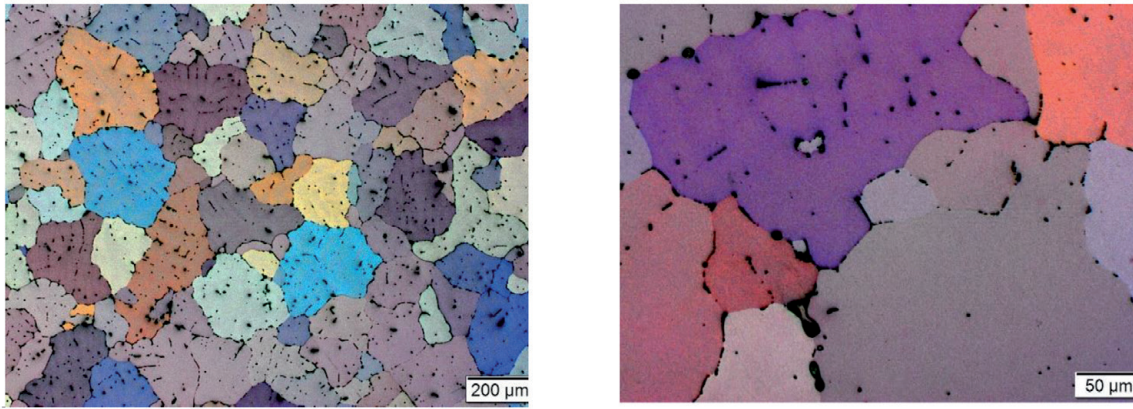
Figure 9.
The structure of Alloy 1 billet with the lowest content of Mg and Si alloying elements.
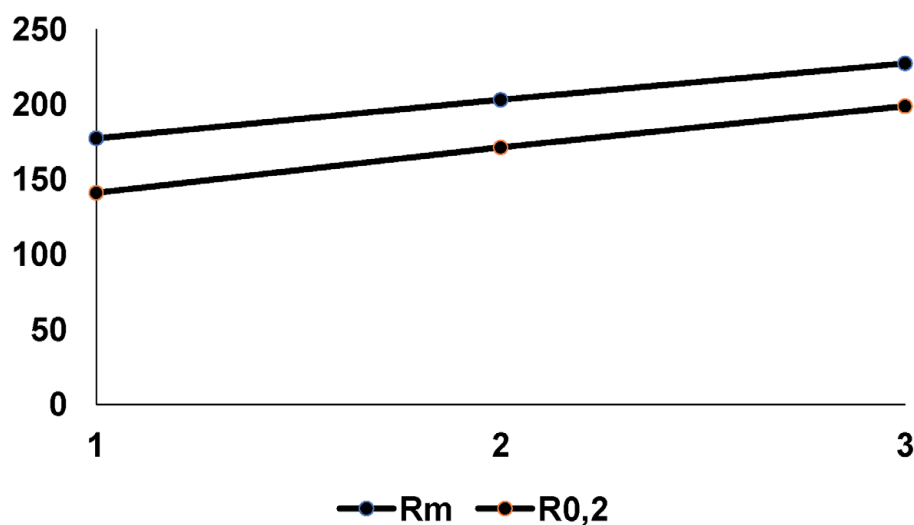

Figure 10.
Yield point and tensile strength of extruded sections from billets with three different contents of the main alloying elements.

Figure 11 illustrates the plasticity of the alloys tested. The highest value of elongation was achieved by the section with the lowest content of alloying elements. This result indicates that the alloy potentially has a plasticity level allowing to use higher extrusion rates in relation to the other alloying components.

The delta (**Figure 11**), i.e., the difference between $R_{0.2}$ and Rm, shown in the diagram (**Figure 11**) illustrates the "yield strength reserve" and confirms the favorable deformation conditions for the alloy with the lowest level of alloying elements with respect to the potential of utilizing its higher plasticity.

The yield point and tensile strength level of Alloy 1 must be achieved by means of a new, finely developed heat treatment.

The next figure (**Figure 12**) shows the elongation of the extruded sections and their hardness. The obtained result confirms that the alloy with the lowest content of alloying elements (Alloy 1) has the highest yield strength reserve.

3.1.3 Studies on the effects of the extrusion rate on the properties, structures, and phase compositions of the alloy with the lowest content of alloying elements

The potential possibility of using the cheapest Alloy 1 with the lowest content of alloying components while optimizing the extrusion rate for the most efficient
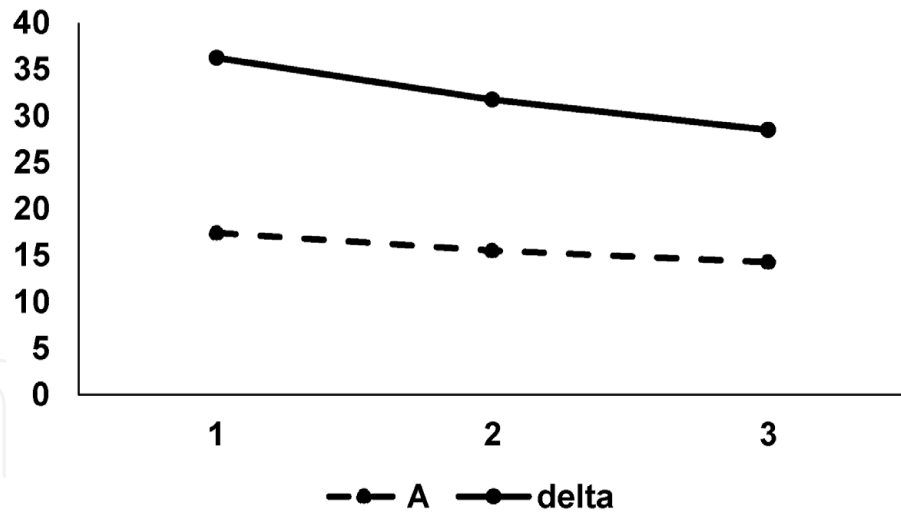
Figure 11.
Elongation and yield strength reserve of extruded sections from billets with three different contents of the main alloying elements.
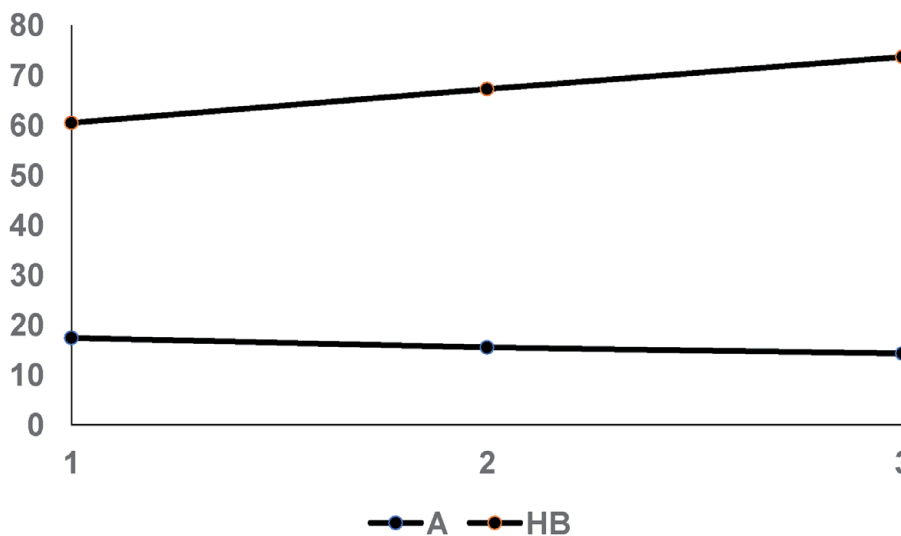

Figure 12.
Elongation and hardness of extruded sections from billets with three different contents of the main alloying elements.

process created grounds for research into heat treatment optimization to achieve the properties required by the standard. Alloy 1 has been tested for its structures, properties, and phase compositions.

Table 5 shows the macrostructure and microstructure of extruded Alloy 1 shapes with respect to the increasing extrusion rate. It is characterized by the equiaxed grains of medium size (medium chord parameter) in the range from 46 μm to 54 μm. Homogenization of the structure and grain size with a maximum grain size difference of 15% results from the hot working, activating the processes of structure recovery during extrusion.

Results of phase composition tests of extruded shapes are presented in **Figure 13**.

There is a final slight decrease in the content of the precipitated phases at the highest extrusion rate applied standard value +60%. At the standard rate +20%, the highest phase content of Mg_2Si and Mg_5Si_6 was recorded. The obtained result sets the direction for actions aimed at obtaining sections with assumed properties at the highest efficiency of the extrusion process. An increase in the extrusion rate above 20%, without changing the subsequent heat treatment applied after extrusion to the
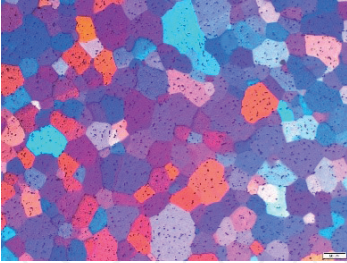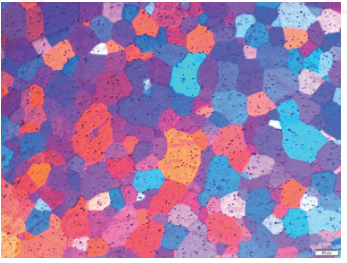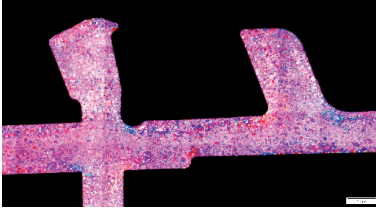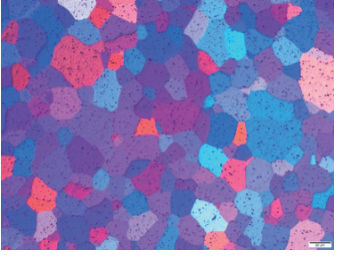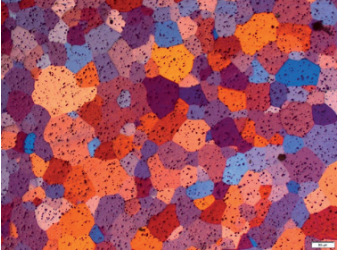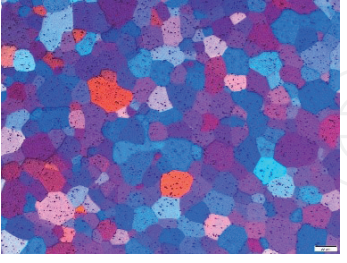
Deformation rate	Section macrostructure	Section microstructure	Grain size, average grain diameter μm
Standard value—X			53
X+20%			46
X+30%			54
X+40%			52
X+60%			48

Table 5.
Structure of Alloy 1 sections depending on the extrusion rate.

T6 state, is an optimal variant ensuring the highest efficiency of the process. On the other hand, if the applied heat treatment allowed for a significant increase in the hardening phase, then higher extrusion rates could be applied.

3.1.4 Effect of heat treatment on the properties of extruded sections made of Alloy 1

The alloy meets the criteria of a high-speed extrusion alloy as the tests resulted in a significant increase in the extrusion rate of sections in relation to the rate currently used. However, due to the low content of Mg and Si alloying elements, the
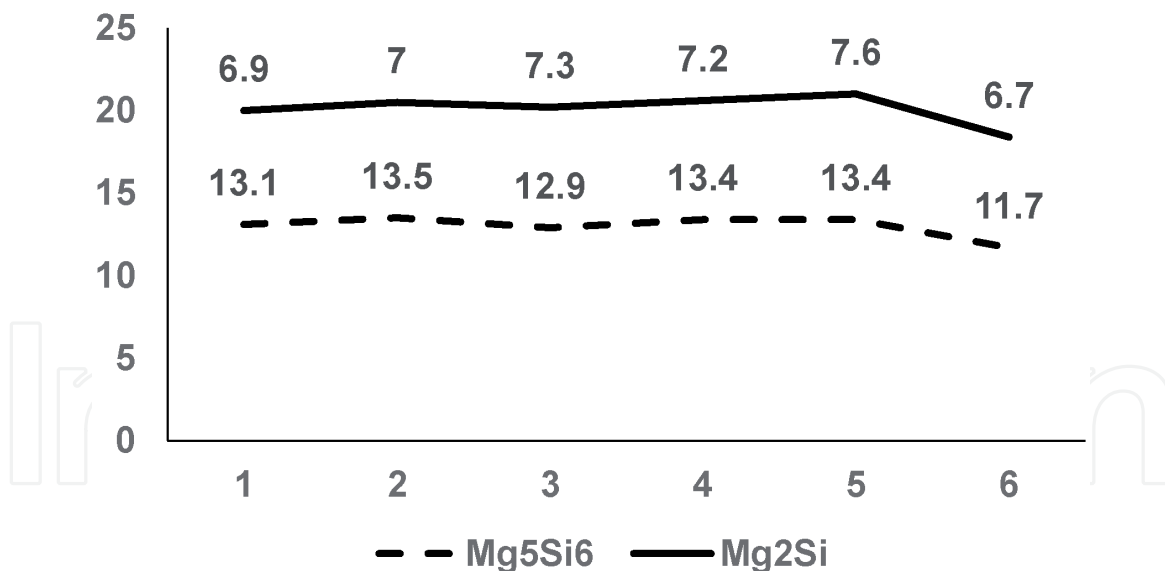
Figure 13.
Phase changes in extruded sections.

Aging curve	Press ram/stem speed	Rm [MPa]	$R_{0.2}$ [MPa]
Aging option 19	Standard value—X	212.0	188.5
	X+20%	218.8	195.3
	X+30%	201.0	176.0
	X+40%	211.0	186.8
	X+50%	200.5	176.3
	X+60%	216.0	183.8

Table 6.
Final results of strength properties after heat treatment for Alloy 1: stage 2.

classical heat treatment did not allow to obtain the recommended level of properties according to the standard. Therefore, it was necessary to carry out a number of studies to develop a new heat treatment that would ensure that the yield point, tensile strength, and hardness value of the standard were achieved. **Table 6** contains data on the parameters of the applied heat treatment variants.

The analysis of the obtained data showed that in variant 19 of heat treatment, the yield point reached the level assumed in the standard. The obtained result is a great technological achievement and promises a better economic result.

The research has shown that it is possible to produce a cheaper alloy (low content of base alloying elements), which allows to use a 60% higher extrusion rate and, using an appropriate heat treatment, achieve a comparable level of properties to alloys containing higher levels of Mg and Si elements.

The higher ductility of the new high-speed extrusion alloy enables the production of a greater tonnage of products per unit of time than the currently used alloys, which translates into increased production efficiency.

4. Summary: 6xxx aluminum alloys for a high-speed extrusion

At the beginning of the twenty-first century, commercial concerns involved in the production and sale of extrusion sections made of aluminum alloys started to show interest in increasing the productivity of the extrusion process through a radical

change in the technology. The subgrades of alloy 6060 with a reduced content of alloying elements, called lean alloys or high-speed alloys, began to form. They were characterized by an increased plasticity in relation to classical alloy 6060, as a result of which the speed of the process increased by 20% in comparison with alloys with classical chemical composition. In order to obtain certain strength properties, it was necessary to use unconventional aging cycles of the material. Because the alloys required an increase in extrusion rate, lean alloys were used primarily for extrusion of sections with relatively uncomplicated cross sections. These types of sections were mainly used in the construction industry, so they were sometimes called building alloys. By 2007, thanks, among other things, to the exchange of workers between the companies, the production technology of building alloys became widely known, and the hydro concern started to produce billets from these alloys for sale to the general public, designing and producing new generations of alloys for fast extrusion at the same time.

Designing alloys for high-speed extrusion requires a deep knowledge of the hardening mechanisms and plastic deformation processes. During hot deformation, which takes place in extrusion, it is important to know the effect of temperature on the extrusion processes. The processes of structure recovery during hot deformation are dynamic recrystallization and dynamic recovery. In aluminum and its alloys, which exhibit high stacking-fault energy, dynamic recovery processes take place.

All effects in the extrusion process are temperature and speed controlled. It is shown that the mechanism of deformation is either dynamic recovery or dynamic recrystallization, according to whether the alloy is of high or low stacking-fault energy. This leads to extrudate structures which contain either subgrains, ideally with no static recrystallization occurring, or grains formed by successive dynamic, metadynamic, and static recrystallization. It is shown that either type of structure is related to, and can be controlled by, the prevailing Zener-Hollomon (Z-H) parameter *Z*. There is thus also a relationship between properties and *Z* [27].

The Zener-Hollomon parameter is given by equation:

$$Z = \dot{e} \backslash \exp(Q/RT) \qquad (2)$$

where $\dot{e}$ is the strain rate, Q is the activation energy, R is the gas constant, and T is the temperature.

The Zener-Hollomon parameter decreases with a decreasing strain rate and an increasing temperature. In the actual industrial production, to avoid the occurrence of cracks, low Z conditions (lower strain rates and higher temperatures) are usually preferred; however, when the deformation rate is too low, the temperature drop is serious, which is harmful for deformation [28].

In case of high-speed extrusion alloys Z-H parameter should increase, the strain rate will increase and temperature should be lowered. The decrease of subgrain/grain size should be expected.

Deformation temperature and strain rate are important factors controlling the hot deformation flow stress. The experimental results show that the dynamic softening is accelerated with the increase of deformation temperature and decrease of strain rate. Strain effects on flow stress and hence on extrusion pressure are predominant for hot extrusion (due to strain rate sensitivity). Therefore, it is rather difficult to predict the extrusion force in hot extrusion. We can estimate the strain rate at any location x in the billet from the geometrical considerations. Let a cylindrical billet have an initial radius of R_o and extruded radius of Rf. be semi-cone angle of the die.

We can formulate the strain rate at any location x from the entry of die as

$$\dot{\varepsilon} = \frac{d\varepsilon}{dt} = -2\frac{v_0 R_0^2}{\left(R_0 - x\tan\alpha\right)^3}\tan\alpha \qquad (3)$$

The average strain rate undergone by a billet is given by

$$\varepsilon = \frac{6v_0 D_0^2 \tan\alpha}{\left(D_0^3 - D_f^3\right)} - \ln R \qquad (4)$$

where v_0 is the velocity of ram.

It is generally believed that the average grain size (D_A) decreases with increasing strain rate and decreasing temperature and is independent of initial grain size and accumulated strain.

The effects of temperature and strain rate can be expressed in terms of the second-order function of the Zener-Hollomon parameter, Z, in an exponent-type function of temperature and strain rate, as follows [29]:

$$D_A = B_o + B_1 \ln Z + B_2 \left(\ln Z\right)^2 \qquad (5)$$

where B_1 and B_2 are polynomial coefficients. Generally, the grain size of as-extruded material decreases with the increase of the Zener-Hollomon parameter. The fact that the Z-H parameter determines the microstructural evolution reveals that the foundation of an ultrafine-grained structure is formed dynamically and the process is closely related to the thermal activation process during and after the deformation.

In general, dynamic recrystallization does not seem to occur in aluminum alloys with Mg below 4%. The high recovery processes develop in such aluminum alloys—with subgrain lattice formation.

The size of stable subgrains that result from dynamic recovery in aluminum alloys depends upon hot working conditions. McQeen et al. [30] expressed this by equation:

$$d_s = a + b \log Z \qquad (6)$$

where d_s is the subgrain size, Z is the Zener-Hollomon parameter, and a and b materials are constant.

The subgrain size usually reaches a limiting value of a few microns in aluminum alloys. With continued deformation, there is usually no further decrease in the subgrain size.

For hot extrusion, the extrusion pressure p is directly proportional to stain rate. As strain rate increases, the extrusion pressure also increases, almost linearly. As ram speed increases, the extrusion pressure also increases, due to increasing strain rate. However, the extrusion pressure is reduced with increased working temperature in hot extrusion (**Figure 14**). The extrusion speed has some limit depending on billet temperature. It means that the technological application of high-speed alloys requires some experimentally developed extrusion parameters.
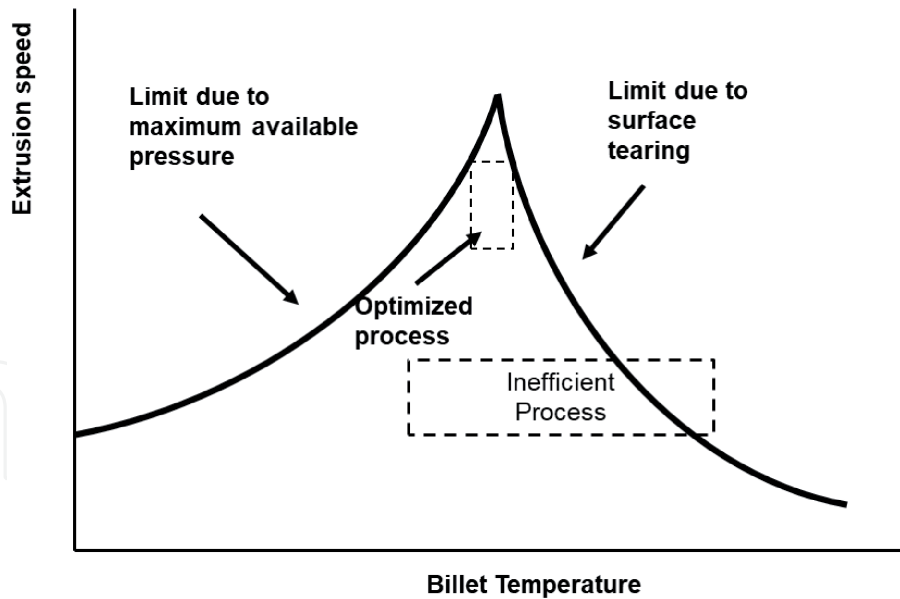
Figure 14.
Temperature dependence to extrusion speed.

In the analysis of hardening of polycrystalline materials, the component (σ_y), described by the model of the Hall-Petch (H-P) equation, acquires a particular importance as it allows to determine the value of lower yield point as a function of grain size:

$$\sigma_y = \sigma_o + k_y d^{-1/2} \tag{7}$$

where σ_y: normal stress corresponding to the yield point; σ_0: stress of internal friction of the mobile dislocations; k_y: slope factor, characterizing the resistance of grain boundaries to dislocation motion; d: diameter of grain or subgrain.

For this reason, the selection of conditions of extrusion rate and temperature determining the grain size is of great importance in the technology of extrusion of aluminum alloys.

At present, high-speed extrusion alloys are a desired alternative to conventional alloys due to the prospect of higher tonnage throughput per unit of time. The expected effect of this action is an increase in the company's profit. In the international literature, it is difficult to find data on the chemical composition of alloys for a high-speed extrusion because they are confidential information, which results from the well-understood interest of the company. There is also a noticeable lack of wider interest of scientists in this subject, who usually strive to disseminate the results, as it is contrary to companies' confidentiality requirements. Therefore, this type of research is usually conducted in a narrow circle of professionals closely cooperating with the industry. Among the literature items and reports that appear on the websites, there is information about progress in the production of new aluminum alloys for specific purposes, e.g., for the automotive, construction, high-speed rail, and other industries. The purpose of the alloys determines their production and properties.

The research conducted on fast extrusion alloys is a promising direction for the development of section production and provides prospects for improving extrusion technology. Great possibilities of increasing the productivity of the extrusion process connected with the implementation of these new quality aluminum alloys are also an element of the struggle for the market and increase in the productivity of companies.

Author details

Rafał Hubicki[1*] and Maria Richert[2]

1 Grupa Kęty S.A., Poland

2 AGH University of Science and Technology, Krakow, Poland

*Address all correspondence to: h_rafal@hotmail.com

IntechOpen

References

[1] Butu M, Moldovan P, Marcu FD, Ungureanu I. Thermodynamics of in situ production of aluminium matrix composites comparative analysis. Materiale Plastice. 2016;**53**(3):428-433

[2] Available from: https://www.azom.com/article.aspx?ArticleID=2863

[3] Marioara CD, Andersen SJ, Zandbergen HW, Holmestad R. The influence of alloy composition on precipitates of the Al-Mg-Si system. Metallurgical and Materials Transactions A. 2005;**36A**:691-702

[4] Vissers R, Van Huis MA, Jansen J, Mariora CD, Andersen SJ. The crystal structure of the β' phase in Al–Mg–Si alloys. Acta Materialia. 2007;**55**(11):3815-3823

[5] Marioara CD, Andersen SJ, Jansen J, Zandbergen HW. Atomic model for GP-zones in a 6082 Al–Mg–Si system. Acta Materialia. 2001;**49**:321-328

[6] Andersen SJ, Zandbergen HW, Jansen J, Traeholt C, Tundal U, Reiso O. The crystal structure of the β'' phase in Al–Mg–Si alloys. Acta Materialia. 1998;**46**(9):3283-3298

[7] Derlet PM, Andersen SJ, Marioara CD, Froseth A. A first-principles study of the β'' phase in Al-Mg-Si alloys. Journal of Physics: Condensed Matter. 2002;**14**:4011-4024

[8] Froseth A. PhD thesis. Trondheim: Norwegian University of Science and Technology; 2003. pp. 63-111

[9] Andersen SJ, Marioara CD, Froseth A, Vissers R, Zandbergen HW. Crystal structure of the orthorhombic U2-Al$_4$Mg$_4$Si$_4$ precipitate in the Al–Mg–Si alloy system and its relation to the β' and β'' phases. Materials Science Journal Engineering A. 2005;**390**(1-2):127-138

[10] Matsuda K, Sakaguchi Y, Miyata Y, Uetani Y, Sato T, Kamio A, et al. Precipitation sequence of various kinds of metastable phases in Al-1.0mass% Mg$_2$Si-0.4mass% Si alloy. Journal of Materials Science. 2000;**35**:179-189

[11] Madsuda K, Ikeno S, Sato T, Kamio A. A metastable phase having the orthorhombic crystal lattice in an Al-1.0mass% Mg$_2$Si-0.4mass% Si alloy. Scripta Materilia. 1996;**34**:1797-1802

[12] Froseth A, Hoier R, Derlet PM, Andersen SJ, Marioara CD. Bonding in MgSi and Al-Mg-Si compounds relevant to Al-Mg-Si alloys. Physical Reviews B. 2003;**67**:224-106

[13] Chakrabarti DJ, Peng Y, Laughlin DE. Precipitation in Al-Mg-Si alloys with Cu additions and the role of Q' and related phases. In: Materials Science Forum. Vol. 396-402. USA: Alcoa Technical Center; 2002. pp. 857-862

[14] Edwards GA, Stiller K, Dunlop GL, Couper MJ. The Precipitation Sequence in Al-Mg-Si Alloys. Acta Materialia. 1994;**46**:3893-3904

[15] Chakrabarti DJ, Cheong BK, Laughlin DE. Automotive Alloys. USA: TMS; 1998. p. 27

[16] Kuroda Y, Yoshino D, Lee SW, Ikeno S, Matsuda K. Microstructure of small amount of TM added Al-Mg-Si alloys with two step ageing. In: Proceedings of 11th Polish-Japanese Joint Seminar on Micro and Nano Analysis, Gniew, September 11-14. 2016. DOI: 10.12693/APhysPolA.131.1373

[17] Zandbergen MW, Cerezo A, Smith GDW. Study of precipitation in Al-Mg-Si alloys by atom probe tomography. II. Influence of Cu additions. Acta Materialia. 2015;**101**:149-158

[18] Takeshi Saito S, Wenner A, Osmundsen CD, Marioara SJ, Andersen J, Royset W, et al. The effect of Zn on precipitation in Al-Mg-Si alloys. Philosophical Magazine. 2014;**94**:2410-2425. DOI: 10.1080/14786435.2014.913819

[19] Lee DH, Park JH, Nam SW. Enhancement of mechanical properties of Al-Mg-Si alloys by means of manganese dispersoids. Materials Science and Technology. 2013;**15**(4):450-455

[20] Chen JH, Constan E, van Huis MA, Xu Q, Zandbergen HW. Atomic pillar-based nanoprecipitates strengthen AlMgSi alloys. Science. 2006;**312**:416-419. DOI: 10.1126/science.1124199

[21] Ringdalen I, Wenner S, Friis J, Marian J. Dislocation dynamics study of precipitate hardening in Al-Mg-Si alloys with input from experimental characterization. MRS Communication. 2017;**7**(3):626-633. DOI: 10.1557/mrc.2017.78

[22] Richert J, Mroczkowski M, Gellner J. Nowy sposób starzenia stopów AlMgSi wyciskanych w stanie T5. Rudy i Metale Nieżelazne. 2006;**51**(12):747-753

[23] Ryen Ø, Holmedal B, Marthinsen K, Furu T. Precipitation, strength and work hardening of age hardened aluminium alloys. Materials Science and Engineering. 2015;**89**:012013. DOI: 10.1088/1757-899X/89/1/012013

[24] Andersen SJ, Marioara CD, Friis J, Wenner S, Holmestad R. Precipitates in aluminium alloys. Advances in Physics: X. 2018;**3**(1):1479984. DOI: 10.1080/23746149.2018.1479984

[25] Available from: https://www.bing.com/images/search?view=detailV2&ccid=V60%2B5rNV&id=019EC72102CAE67AB922781ADE5BCA40109097CB&thid=OIP.V60-5rNVOMKKmWU8zuw79gHaFf&q=mg2si+precipitations+in+6060+alloy&simid=608017416757841339&selectedindex=1&mode=overlay&first=1

[26] Grupa Kęty S.A. Photos by authors.

[27] Sheppard T. Temperature and speed effects in hot extrusion of aluminium alloys. Metals Technology. 1981;**8**(1):130-141. DOI: 10.1179/030716981803276009

[28] Li J, Liu B, Wang Y, Shan T, Liu Y, Lu X. A study on the Zener-Hollomon parameter and fracture toughness of an Nb-particles-toughened TiAl-Nb alloy. Metals. 2018;**8**(4):287. DOI: 10.3390/met8040287

[29] Quan G-z, Wang Y, Liu Y-Y, Zhou J. Effect of temperatures and strain rates on the average size of grains refined by dynamic recrystallization for as-extruded 42CrMo steel. Materials Research. 2013;**16**(5):1092-1105. DOI: 10.1590/S1516-14392013005000091

[30] McQeen HJ, Celliers OC. Application of hot workability studies to extrusion processing: Part II. Microstructure development and extrusion of Al, Al-Mg and Al-Mg-Mn alloys. Canadian Metallurgical Quarterly. 1996;**35**(4):305-319